Neurite Guidance and Three-Dimensional Confinement *via* Compliant Semiconductor Scaffolds

Francesca Cavallo,*,†,§ Yu Huang,‡,§ Erik W. Dent, Justin C. Williams, and Max G. Lagally

University of Wisconsin—Madison, Madison, Wisconsin 53706, USA. §These authors contributed equally to this work. †Present address: University of New Mexico, Albuquerque, NM 87106, USA. ‡Present address: Houston Methodist Hospital Research Institute, Texas Medical Center, Houston, TX 77030, USA.

ABSTRACT Neurons are often cultured *in vitro* on a flat, open, and rigid substrate, a platform that does not reflect well the native microenvironment of the brain. To address this concern, we have developed a culturing platform containing arrays of microchannels, formed in a crystalline-silicon nanomembrane (NM) resting on polydimethylsiloxane; this platform will additionally enable active sensing and stimulation at the local scale, *via* devices fabricated in the silicon. The mechanical properties of the composite Si/compliant substrate nanomaterial approximate those of neural tissue. The microchannels, created in the NM by strain engineering, demonstrate strong guidance of neurite outgrowth. Using plasma techniques, we developed a means to coat just the inside surface of these channels with an adhesion promoter (poly-D-lysine). For NM channels with openings larger than the cross-sectional area of a single axon, strong physical confinement and guidance of axons through the channels are observed. Imaging of axons that grow in channels with openings that approximate the size of an axon suggests that a tight seal exists between the cell membrane and the inner surface of the channel, mimicking a myelin sheath. Such a tight seal of the cell membrane with the channel surface would make this platform an attractive candidate for future neuronal repair. Results of measurements of impedance and photoluminescence of bare NM channels are comparable to those on a flat NM, demonstrating electrical and optical modalities of our platform and suggesting that this scaffold can be expanded for active sensing and monitoring of neuron cellular processes in conditions in which they exist naturally.

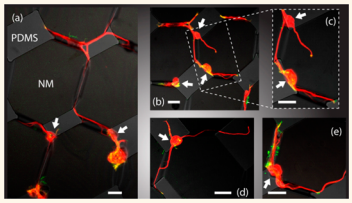

KEYWORDS: buckled nanomembrane scaffold · compliant substrate · single neuron · guidance · 3D confinement

A wealth of applications in the field of neuroscience and neuroprosthetics[1−4] will benefit from hybrid neural electronic/photonic systems to investigate neural processes and neuron−neuron interactions and to achieve controlled stimulation/readout of cell activity. However, in spite of all the efforts directed to build neural culture scaffolds and neuroprosthetic devices,[1,4−13] a successful integration of devices and cells on the same substrate is still far from reality. Coupling between biological tissue and a solid-state device can be established through chemical, electrical, or optical signals and through their mutually exerted mechanical forces. Although bio/inorganic interactions have been widely viewed from electrical, optical, or chemical standpoints, mechanical compatibility has been infrequently considered. In our work, we focus on this aspect of neurodevice integration.

A major challenge in this regard derives from the high elastic-properties mismatch between the microenvironment of neurons and traditional culture platforms and device substrates. For instance, the elastic modulus of a central nervous system (CNS) environment is on the order 0.1−10 kPa,[14] whereas metals, semiconductors, and other materials commonly used as culture substrates have elastic moduli in the range of 1−200 GPa.[15] This large discrepancy in mechanical microenvironments affects neuronal development, outgrowth, and migration, even altering neuron cell features and functionality.[16−20] What is therefore needed, in contrast to the use of traditional cell culture (*e.g.*, glass, polystyrene) or semiconductor device materials (*e.g.*, bulk single-crystal Si and SiO_2), is a compliant substrate that enhances material−cell contact and preserves the physiological condition of cells/tissues, while enabling electronic/photonic sampling, sensing, and stimulation.

A second challenge concerns stimulation or probing of single neurons with high signal-to-noise ratio (SNR). Neurons can be

* Address correspondence to fcavallo@unm.edu.

Received for review July 19, 2014 and accepted December 5, 2014.

Published online December 05, 2014
10.1021/nn503989c

stimulated by electrodes that are capacitively coupled to the cell membrane to change their potential[21] or for genetically modified cells containing light-sensitive channels by photonic devices emitting in the visible range.[22] In both cases, close proximity of the stimulating device to individual neurons is required to guarantee neuronal activation with high spatial resolution and SNR. The electric activity of individual neurons may also be recorded by electrodes or field-effect transistors (FETs) adjacent to the cell body or its processes.[21,23] The amplitudes of action potentials to be measured are very small (~40 μV) and decay rapidly away from the cell, becoming easily overwhelmed by background noise.[24,25] In an ideal scenario, photonic devices and electrodes should be in close contact and compliant with the neuronal membrane. Furthermore, the cell/device interface should ideally be electrically isolated from nearby cells to maximize the SNR.

We describe here a nanomaterial approach with the potential of overcoming these limitations. In an earlier work,[26] we have shown that the mechanical properties of crystalline-semiconductor nanomembranes (NMs)[27−29] bonded to compliant substrates can be tailored to match those of cell microenvironments, including the CNS environment. Yet such semiconductor NMs easily retain all the properties required for fabrication of sensing, amplification, and stimulating devices.[27−29]

In the following, we overview the fabrication of topographically patterned NMs on polydimethylsiloxane (PDMS), demonstrate neurite guidance through and on the fabricated structures, and show integration of electrical and optical functionalities in the buckled channels. A consequence of the exceptional compliance of NMs is the ability to define ordered 3D microarchitectures, in particular, here micron-size channels, fabricated using ultrathin crystalline-silicon sheets (Si nanomembranes, SiNMs) on an elastomeric substrate, PDMS.[30] (We have also made microarchitectures on even more compliant substrates; see Figure S1 in the Supporting Information.) These channels, created by strain engineering of the above combination, are arranged into ordered 2D arrays, with amplitudes ranging from ~10 to ~1.5 μm, sizes comparable to the diameter of a typical neurite (we use "axon", "neurite", and "neuronal process" interchangeably throughout this paper). Combining a novel plasma-based approach to coat the inside of the microchannels, we show that primary cortical neurons interact specifically with these channels. We demonstrate strong physical confinement and guidance of single neuronal processes through them.

Conversely, we show that, if NM channels have smaller openings than the dimension of a single axon, neuronal cells send processes on top of the NM channels, preferentially along the channel axis. We compare chemical and topographic guidance.

Other types of biomaterial scaffolds exist as alternatives to commonly used substrates for cell culture, such as glass and polysterene. It is worth noting, however, that our NM scaffold is made completely of silicon, a widely studied nontoxic semiconductor. In contrast to other scaffolds, given the optical and electrical functionalities of the NM system, it is not unrealistic to anticipate the integration of this platform with microelectrodes in the use of neuroprosthetics.

RESULTS AND DISCUSSION

Patterned Substrates. We perform cell cultures on two different types of substrates: (1) single-crystal SiNMs, bonded on PDMS, patterned in a 2D array of rectangular islands connected by buckle-delaminated 3D channel structures; and (2) single-crystal SiNMs patterned in stripes (Si nanoribbons, SiNRs) and formed into periodic parallel wrinkles (1D) on close-to-coherently deformed PDMS substrates. The fabrication of 3D structures on hard/soft substrates and the mechanics and chemistry underlying the process are detailed in our earlier work.[30] In brief, a SiNM is transferred onto a PDMS thin substrate and patterned. The PDMS support is then swollen in an organic solvent. Evaporation of the solvent causes the PDMS to recontract and create mechanical strain, which eventually leads to local and periodic buckling delamination of the SiNM.

Our technique allows fabrication of any desired number of buckle-delaminated structures arranged in various fashions, with different in-plane separations, by selecting patterns with connected bonded regions ("islands") of appropriately defined shapes. The relative arrangement of the buckle-delaminated structures is controlled by the shape and arrangement of the interconnecting sections of the NM. Figure 1a−d shows top-view optical images of buckle-delaminated channels arranged in various fashions on the PDMS surface. For example, in Figure 1a,d, 72 nm thick SiNMs are formed into four buckled-up channels of similar length but different channel widths, as defined by the relative distance of the interconnects. Bare PDMS regions from which six and eight channels emanate are obtained by patterning hexagonal and cross-shaped holes arranged in a near-checkerboard fashion (see Figure 1b,c).

As a second category of 3D microtopography, linear arrays of wrinkled (as opposed to buckle-delaminated) NM structures can be fabricated, as described in the Materials and Methods section. Figure 2 shows images of wrinkled NM structures and their scalability with strain. When wrinkling occurs, the PDMS substrate close-to-coherently deforms along with the NM.[30−32] As a result, the open area between the NM and the substrate is significantly lower than for buckle-delaminated channels, for which the PDMS remains flat. The origin of this mechanical instability is discussed in our earlier work.[30]

Figure 2c illustrates the behavior of out-of-plane dimensions (*i.e.*, amplitude *versus* length) of wrinkled

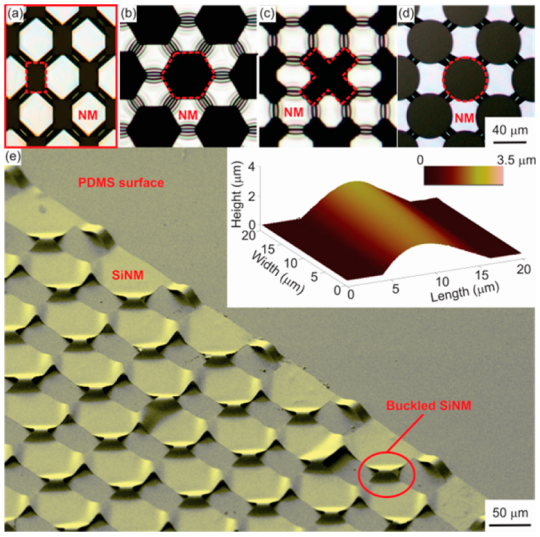

Figure 1. Effect of NM pattern on number and arrangement of buckle-delaminated channels. (a–d) Top-view optical images of 2D arrays of ordered buckled channels formed by NM/PDMS immersed in acetone for 2 h, rinsed in isopropyl alcohol for 120 s and exposed to air for 15 min. From left to right, buckles of different widths are shown (see inset for definition of length and width). Two-dimensional arrays of buckled channels are obtained by patterning the NM in a near-checkerboard pattern with rectangular islands connected by narrow portions of the NM. The SiNMs in a–d and b–c are 72 nm and 17 nm thick, respectively. (e) Tilted SEM image showing 72 nm thick SiNMs formed into buckled channels at the interconnects of the near-checkerboard pattern. The inset shows a 3D AFM image of a single buckle-delaminated channel formed by a 72 nm SiNM.

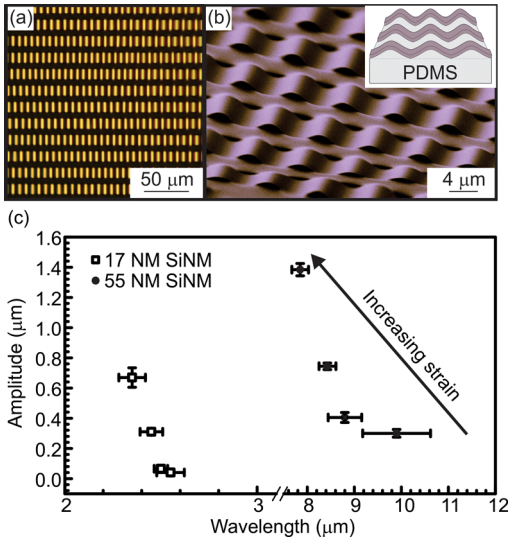

Figure 2. Microscopy images of a wrinkled (as opposed to buckle-delaminated) NM/PDMS system, upon treatment in different solvents, and scalability of wrinkling with NM thickness and applied strain. (a) Top-view optical image and (b) tilted off-axis SEM image of a periodic array of 55 nm thick wrinkles after 20 h immersion in acetone and 15 min exposure to air at room temperature. The inset illustrates schematically linear arrays of wrinkled structures in Si/PDMS. (c) Scalability of the wrinkled structures with thickness and applied strain. Different values of applied strain are obtained using different solvents, as described in the Materials and Methods section. The plot shows that various combinations of NM thicknesses and applied strain can be used to tune the amplitude and spacing of wrinkled structures.

structures as a function of applied strain. The two data sets in Figure 2c correspond to 17 and 55 nm thick NM/PDMS systems, treated with several solvents for 20 h (although no further swelling of the PDMS substrate occurs after 2 h[30]). Each solvent produces a different degree of swelling of the PDMS and hence a different value of strain applied to the SiNM during deswelling.[30]

Neurite Guidance. We access neurite guidance using a primary mouse cortical cell culture, a commonly used *in vitro* model. We initially verify cell viability in the fabricated structures, as any residual organic solvent from the template fabrication process may damage neurons, even though the individual raw materials, silicon and PDMS, are intrinsically not cytotoxic. All scaffolds support healthy neural growth for 2 weeks, as judged by cell morphology, cytoskeletal immunostaining, and membrane integrity (see Figure S2 in the Supporting Information). This outcome suggests that the solvent extraction step has thoroughly depleted solvents to benign levels. Additionally, all scaffolds are functionalized with poly-D-lysine (PDL) to ensure proper adhesion of neurons to the inorganic substrate.[33,34] The details of this procedure are described in the Materials and Methods section; they vary slightly depending on the sample type, as detailed below for each experiment.

Neurons at a low density (~500 cells/cm^2) are seeded on the hard/soft substrates to ensure that overlapping cell growth does not affect guidance. After 5 days *in vitro*, cell cultures were immunostained with antibodies against actin and tubulin and subsequently imaged with upright confocal microscopy. Tubulin and actin are labeled to capture the neurite and small filopodium processes, respectively. This approach is used to confirm 3D confinement of the cell process inside the buckle-delaminated channels.

Figure 3 shows the neural culture results on substrates with 2D arrays of buckle-delaminated channels. The inside of the NM channels is functionalized with PDL to promote adhesion of neurons in proximity of the channels and achieve neurite guidance by the buckled NMs. Selective PDL coating in the 3D scaffolds is achieved by spin-coating a uniform layer of PDL on the combination substrate and performing a transient oxygen plasma etch at low RF power. The key concept is that during this oxygen plasma step the diffusion of the etching gas in the NM channel is limited by the low power and the short duration of the etching process. As a result, the PDL is removed everywhere on the sample surface except in the buckle-delaminated channels. The seeded individual neuronal soma (cell body) adheres on the unfunctionalized PDMS surface in the vicinity of the inlets to SiNM channels and extends processes through the channels. Robust guidance is observed both for a single neurite growing

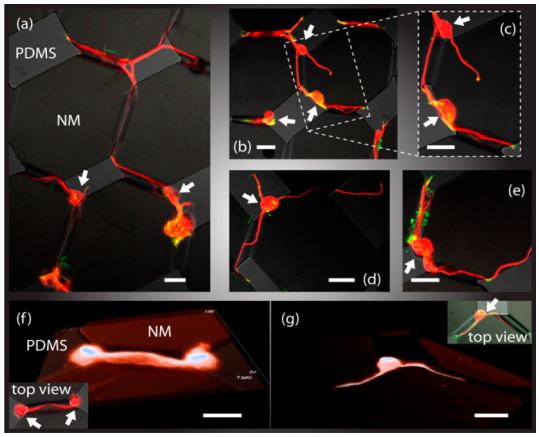

Figure 3. Confocal fluorescence microscope images showing strong guidance of neuronal outgrowths by buckle-delaminated channels, while excluding the neuronal cell body (indicated by arrows). Neuronal processes have been observed to be guided through up to five channels (a) and to form putative networks with each other (b,c), whether the cell is multipolar (d) or bipolar (e). Three-dimensional rendering of confocal images confirms that neuronal processes are confined inside the channel for both a putative network (f) and a single cell (g). The channels are formed by 72 nm thick SiNMs on PDMS after immersion in acetone for 2 h, rinse in isopropyl alcohol for 120 s, and subsequent 15 min exposure to air at room temperature. The measured amplitude of the channels is ~3.5 μm. Actin is labeled in green. Tubulin is labeled in red. Tubulin and actin are labeled to capture neurites and small filopodium processes, respectively. Scale bar in all cases: 20 μm.

serially through multiple scaffolds (see Figure 3a) and for multiple cells extending neurites into and through a single channel (see Figure 3b,c), for both multipolar (Figure 3d) and bipolar neurons (Figure 3d,e). On the other hand, no guidance is observed on samples uniformly coated with PDL, as shown in Figure S2 in the Supporting Information. In contrast, guidance is also observed for unfunctionalized tubes if a PDL pad is provided at the tube opening for adhesion of the soma.[34] Three-dimensional rendering of the confocal microscope images confirms that neurites are spatially confined inside the buckle-delaminated channels (Figure 3f,g). Figure 3f shows the cytoskeletal structure of two single neurons that grow toward each other, guided through a single channel. The processes of these neurons appear to branch inside the channel, extensively interact with each other, and even generate putative synaptic contacts. The above results confirm that an appropriately functionalized substrate with buckle-delaminated SiNM channels can effectively support neural culture, guide neurite outgrowth, and form putative neuron networks in various patterns.

We observe that neurites confined within the buckle-delaminated channels have a strong tendency to grow along an inside edge of the channel, an interesting phenomenon that has not been commonly observed in other confined-guidance cues, such as rolled-up tubes[34,35] with circular cross sections or microfluidic channels with flat tops.[36] Our observation may be explained by the uniquely bell-shaped cross-sectional area of NM channels, where the space near the channel edge is significantly more confined than at the center and therefore provides enhanced cell surface contact.

Turning now to the linear arrays of wrinkled structures shown in Figure 2 (as opposed to the buckle-delaminated structures shown in Figure 1), we find two distinct guidance effects. These are dependent on the size of the opening of the channel formed by the buckled NM. Figure 4a shows four channels in a 55 nm SiNM that appear similar to buckle-delaminated structures but are created by interfacial defects.[30] The channels are ~10 μm long but with an amplitude of only ~1.5 μm, much lower than the ~3.5 μm amplitude of the deliberately buckle-delaminated channels shown in Figure 1 and used in the results shown in Figure 3. The Materials and Methods section describes how these wrinkled structures are characterized. Because the amplitude is less, the cross-sectional area available for neurite outgrowth is smaller than for the channels in Figure 3. In Figure 4a, neurite guidance through the NM channels is shown, similarly to that observed for the larger channels shown in Figure 3. However, the relatively small size (with amplitude comparable to the diameter of axons) of the channels in Figure 4a results in neurites being spread evenly throughout the entire channel space instead of being restricted to the channel edge, as they predominantly are in Figure 3. In addition, the spatial confinement of the cell within the channel is tight, judging by the absence of tubulin antibody staining (red color) in the middle of the channel. The apparent exclusion of these types of macromolecules from the intracellular space suggests that a tight seal exists between the cell membrane and the inner surface of the channel. Such a tight seal of the cell membrane with the channel surface would make our device an attractive candidate to mimic myelin, whose tight enclosure around the axon is crucial to salutatory propagation, a key process that maintains efficient nerve communication.[37] For future application of this flexible neuro-electrode interface, close contact would also provide the neuron process with protection from an immunoresponse and better potential signal transfer with electrodes.[21,23,24] Furthermore, the 3D confinement provided by the scaffolds is commonly believed to increase cytoskeletal tension of the growth cone, a desirable feature to guide axon extension or branching, similar to the native topographic environment (*e.g.*, myelin, packed interstitial space) of CNS.

We also culture neurons on a 55 nm thick SiNM that has formed wrinkles on PDMS (*i.e.*, where the PDMS coherently deforms along with the NM).[30] In these samples, the open area between the NM and the supporting wrinkled PDMS substrate is on the order of a few hundred nanometers, that is, much smaller than

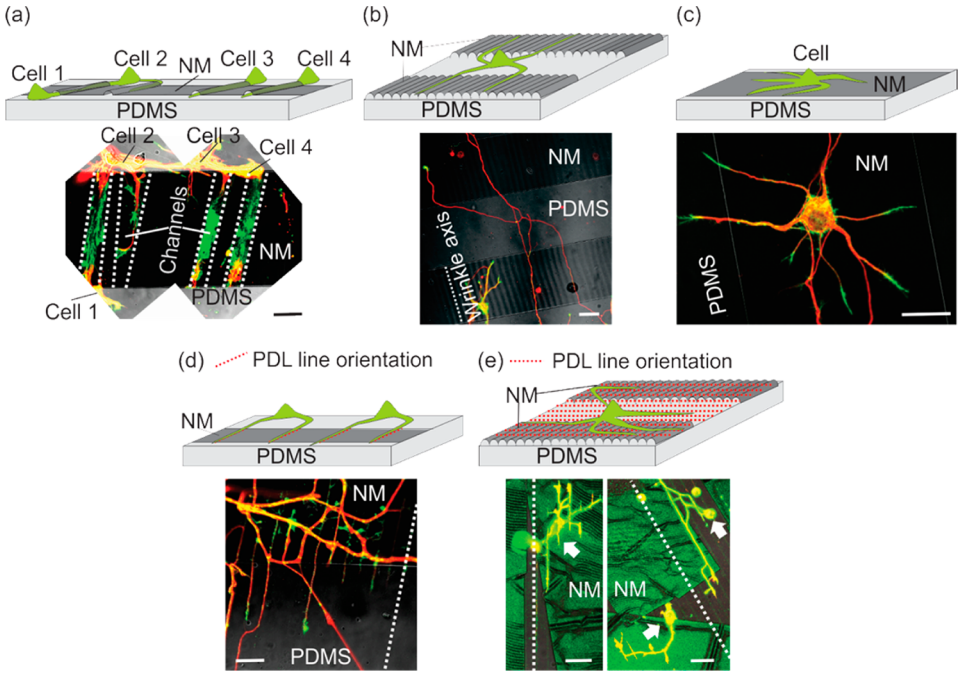

Figure 4. Schematic illustration and confocal optical microscope images of neural growth in or on periodic arrays of buckle-delaminated or wrinkled NMs. (a) Linearly arranged buckle-delaminated NMs three-dimensionally confine and guide neuronal processes. In (a), the dotted lines mark the edges of four channels. The sample in (a) was functionalized as described in the Materials and Methods section to obtain a PDL coating inside the channel only. (b) Wrinkled NMs guide neurites along their axis because of topography. The dotted line marks the direction of the wrinkle axis and of the guided processes. (c) No such guidance is exhibited by the flat NM on PDMS. The samples in (b,c) were uniformly coated with PDL. (d) Micropatterned PDL lines applied to the flat NM. (e) Micropatterned PDL lines applied to wrinkled NMs. In (d,e), neuron processes are guided by the PDL lines. The dotted lines specify the direction of the micropatterned PDL lines. Scale bar equals 15 μm in all cases.

the axon dimensions. As a result, neurite outgrowth between the NM and the PDMS substrate is prevented. In order to investigate any topographic guidance of the neurites by the wrinkled NMs, the samples are uniformly coated with PDL. Figure 4b shows that, similar to the topographic guidance provided by commonly studied substrate topographies of comparable dimension,[36,38] neurite outgrowth on wrinkles (Figure 4b) displays a parallel guidance (preference to grow along the topographic feature). In contrast, outgrowth on the control substrate (*i.e.*, a flat NM/PDMS uniformly coated with PDL) displays no preferred guidance.

In addition to the topographic guidance provided by the periodically arranged wrinkles, we also explored guidance effects of a combination of periodic wrinkled structures and micropatterns of adhesion molecules. Instead of coating PDL uniformly over a large area, we deposited 8 μm spaced and ~1.6 μm wide PDL stripes onto the flat (Figure 4d) or wrinkled (Figure 4e) NM surfaces by microcontact printing.[11] The subsequent neurite outgrowth follows the PDL stripe pattern on both the flat NM and the PDMS (see Figure 4d), similar to what has been previously observed,[11] suggesting that adhesion-based guidance is viable with our SiNMs. For comparison, we applied the same PDL pattern perpendicular to the periodic wrinkled structures, whose topography alone induces a guidance parallel to the wrinkle ridges/grooves. As shown in Figure 4e, the neurites now predominantly followed the PDL pattern, suggesting that chemical (adhesion) guidance has a higher hierarchy than that of topography.

The 3D topography provided by wrinkles (ridges or grooves) may enhance a neurite's cytoskeletal tension, as for the filled channels, even though the guidance effect should be much weaker because of the lower level of confinement. However, without the presence of any other guidance cue, the neurites follow the wrinkle ridge direction. With a stronger adhesion guidance cue, the weaker guidance of topography is ignored.

Electrical and Optical Modalities. Finally, we demonstrate that both electrical and optical functionalities can be integrated in a buckle-delaminated NM, with the potential to stimulate or probe electric activity of neurons. In these experiments, the scaffolds were not coated with PDL as we expect that a coating of PDL could not change the outcomes of what is shown here.

Figure 5a shows four buckle-delaminated channels formed by a 42 nm thick SiNM on PDMS. Rectangular contact pads are fabricated on the NM prior to its release and transfer to the PDMS substrate, using conventional patterning and deposition techniques, as described in the Materials and Methods section. Immersion in solvent does not affect the contact pads, leaving them planar and well-adhered to the SiNM surface. A typical $I-V$ curve for a buckled NM/PDMS

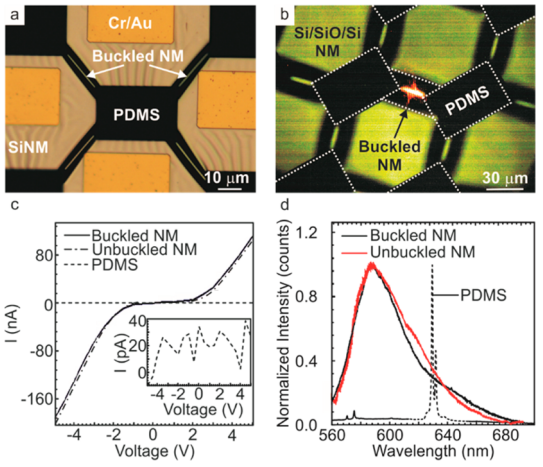

Figure 5. Buckle-delaminated NMs as electrical interconnects and light emitters. (a) Top-view optical image of a 42 nm SiNM formed into four buckle-delaminated channels at the interconnects of rectangular areas of PDMS, labeled as "Buckled NM". Four rectangular-shaped 5 nm Cr/200 nm Au contact pads are fabricated on the NM prior to NM release and treatment in solvents. (b) Top-view optical image of an annealed 10/10/10 nm Si/SiO/SiNM formed into buckle-delaminated channels at the interconnects between rectangular areas of PDMS. Photoluminescence spectra are acquired for the buckled film using a laser beam focused to a ~3 μm diameter laser spot (orange colored), as shown in (b). The edges of the photoexcited buckled channel and the rectangular holes in the NM are marked by dotted lines. (c) Typical current–voltage characteristics measured for the NM between the contact pads before (solid line) and after (dash-dotted line) buckling has occurred. Schottky contacts between the undoped NM and the contacts cause the threshold behavior. The inset shows the *I*–*V* curve measured between contact pads on bare PDMS. The current fluctuates in the range of few tens of pA, indicating that no low-resistance parasitic path exists on the PDMS substrate. (d) Typical photoluminescence spectra acquired from the annealed 10/10/10 nm Si/SiO/SiNM and the bare PDMS. PL spectra for both an unbuckled (red solid line) and buckled (black solid line) NM are shown. Broad spectrum luminescence is attributed to Si nanoclusters in the oxide matrix and radiative defects at the nanoclusters/oxide interface.

structure is shown in Figure 5c. Schottky contacts between the p-SiNM and the deposited Cr/Au are responsible for the threshold-like behavior in Figure 5c. An average resistivity on the order of 4 ± 0.5 Ωcm is inferred from the ohmic region of the *I*–*V* curves measured for 10 different buckled structures on the same sample. A comparable resistivity is calculated from the *I*–*V* characteristics measured for the films prior to buckling (see dash-dotted line in Figure 5c). Four-probe measurements across the SOI wafer prior to NM fabrication yield values of 2 ± 0.3 Ωcm, suggesting that the fabrication process, including treatment in solvent, has little effect on the NM electronic conductivity or the integrity of the electrical contact between the Cr/Au film and the NM. The *I*–*V* response acquired between two contact pads on PDMS is also shown, in the inset of Figure 5c. A measured current fluctuating in the range of a few picoampere excludes the existence of a low-resistance parasitic path in the PDMS substrate. In our experiments, low current values are obtained because we use undoped NMs. However, our approach can be applied to NMs that are uniformly doped to achieve a higher current flow.

Next, we demonstrate that our approach can be applied to NMs containing light-emitting elements. For this purpose, we deposit a symmetric multilayer stack including 10 nm of amorphous Si (a-Si)/10 nm SiO/10 nm a-Si on 400 nm a-Ge on a handle Si substrate. The a-Ge and a-Si/SiO/a-Si films serve, respectively, as sacrificial and functional layers. The NM is then patterned in a checkerboard fashion and undergoes rapid thermal annealing at 800 °C for 30 min. Annealing promotes the formation of Si nanoclusters in the SiO matrix, which produce photoluminescence (PL) in the visible range.[39,40] The Si/SiO/SiNM is released by selective removal of the Ge sacrificial layer, *via* etching in (31 vol %) H_2O_2 at room temperature. After dry transfer to a PDMS substrate, the combination Si/SiO/SiNM/PDMS system is immersed in acetone for 30 min and rinsed in isopropyl alcohol (IPA) for 120 s. As the solvent evaporates, the multilayered NM buckles at the interconnects, in the same manner as the SiNM. Figure 5b shows a top-view optical image of the NM formed into rectangular regions interconnected by buckle-delaminated structures. We measure PL from the films in the buckled areas using a 633 nm laser source focused to a ~3 μm spot on top of a buckle-delaminated area, as shown in Figure 5b. Typical PL spectra obtained from the film before and after buckling are shown. For comparison, PL acquired from the bare PDMS surface is also plotted. A broad spectrum centered at ~590 nm is acquired from the NM at the interconnects before immersion in solvent. No changes in the peak emission wavelength or the maximum intensity of the PL spectrum are observed after subsequent fabrication of the 3D scaffolds (buckle delamination), confirming that the fabrication process, including solvent treatment, is not detrimental to the mechanism responsible for the PL. Figure 5b shows that our technology allows integration of room temperature light emitters in a 3D scaffold for neuron culture. This result has significant implications for the rapidly developing field of optogenetics.[22] In optogenetics, genetically modified neurons are activated or silenced by light stimuli at specific wavelengths in the visible spectrum. Successful experiments have been conducted using 470 and 590 nm as excitation wavelengths. More recently, researchers have used other channels that enable red light to excite/inhibit specific groups of neurons.[41,42] In this scenario, 3D confinement of neurons by channels formed by optically active NMs may enable delivery of the light stimuli with a high degree of specificity and spatial resolution. A further advantage of our process is the capability of tuning the luminescence spectra acquired from the NM to match all the specific wavelengths used to control cell activity.[39–43]

CONCLUSIONS

When crystalline materials are fabricated with at least one dimension in the nanoscale, their mechanical properties become significantly different from those of corresponding bulk material. In the present context, if that thin sheet is a semiconductor, it retains all its valuable signaling and sensing functions, while making its mechanical properties compatible with biological environments, thereby creating an ideal fit for investigations in neuroscience. We have successfully used strain engineering of silicon-based NMs to pattern 3D microscale structures on a compliant substrate with sizes that match cellular dimensions. By themselves, these structures provide topographic guidance for individual neuronal growth/outgrowth, through either channel confinement or an underlying wrinkle topography, providing in some situations configurations that mimic a myelin sheath. The electrical and optical modalities of these semiconductor NMs are also preserved in these 3D structures through all the required processing steps. With these unique features, our NM platform makes an ideal neural interface substrate, with high resolution, high signal-to-noise ratio, and high compliance, thereby addressing and overcoming prominent existing challenges.

MATERIALS AND METHODS

Nanomembrane Fabrication and Transfer to the Compliant Host. Two-dimensional and linear arrays of buckled structures on PDMS are fabricated using SiNMs with thicknesses varying between 17 and 270 nm. Silicon-on-insulator (SOI) wafers, consisting of a 150−270 nm thick Si template, a 150−3000 nm-thick buried oxide (BOX) layer, and a bulk Si handle layer, are used as starting substrates. Thinner Si templates are obtained by thermally oxidizing the starting substrates and removing the SiO_2 grown in an HF (49 vol %) solution. The thickness of the NM is measured by X-ray diffraction or reflectometry. SiNMs are patterned in 20−100 μm wide stripes with a 20−100 μm pitch to fabricate linear arrays of buckled structures. Networks of buckle-delaminated channels are obtained by patterning NMs in a checkerboard fashion with rectangular-shaped holes. The lateral size of the SiNMs varies between 0.4 × 0.4 and 1 × 1 cm^2. Patterning of the Si templates before release is achieved by optical lithography and reactive ion etching with SF_6/O_2. SiNMs are released from the SOI wafer by selectively etching the BOX in the SOI wafer using HF (49 vol %). After complete removal of the BOX, two different techniques are used to transfer the released NMs to PDMS. In one case, the SiNMs are floated off in deionized water and transferred onto the PDMS. In the other case, the NMs are released, allowed to rest on the original substrate (*i.e.*, the Si handle wafer), where they bond only weakly, and subsequently peeled off using the PDMS substrate.[28−30]

Fabrication of PDMS Substrates. The PDMS substrate is prepared by casting a liquid PDMS mixture (10:1 weight ratio of silicone elastomer to curing agent, Sylgard 184, Dow Corning) onto a chemically cleaned Si wafer and curing for 4 h at 85 °C. The cured PDMS sheet is approximately 2 mm thick. Immediately before bonding to the NM, the PDMS sheet is peeled off the Si wafer and surface-activated by an oxygen plasma for 30 s at a power of 50 W. Solvents are obtained from Sigma-Aldrich Co. (St. Louis, MO), Fisher Scientific Co. (Pittsburgh, PA), and VWR (Radnor, PA) and used as received.

Fabrication and Characterization of 2D and Linear Arrays of Buckled Structures. SiNMs are transferred to the plasma-treated PDMS substrate immediately after their release from the SOI and, after a delay of ∼20 h, immersed in solvent. The purpose of the delay is to allow any water trapped between the NM and the substrate to diffuse out of the interface. The purpose of the plasma treatment of the PDMS prior to NM transfer is to present a more reactive surface to the NM.[30] Treatment in solvent is performed in glass beakers at room temperature. The duration of the treatment is ∼20 h. We used *N*-methylpyrrolidone (strain, ε = 0.9%), methanol (strain, ε = 1.5%), IPA (strain, ε = 3.7%), and acetone (strain, ε = 7.2%).[30] The values of applied strain are calculated from the measured swelling ratio, *S*, of the PDMS in solvents, as described in ref 30. Controlled buckling of the NM is then achieved by exposing the sample to air, with solvent evaporating at room temperature. Measurements on the 17 and 55 nm SiNM/PDMS systems undergoing the process illustrated in ref 30 show periodic wrinkles on the substrate surface for all levels of applied strain. Along with ordered wrinkles, we observe occasional buckle delamination of the NM in localized areas and formation of channels with a relatively large opening (∼1.5 μm), but still much smaller than the openings in deliberately buckle-delaminated channels (∼4−10 μm). We attribute the formation of these channels to defects at the NM/PDMS interface (*e.g.*, particles) between the NM and the PDMS. Particles result in a pre-existing interfacial delamination that expands when compressive strain is applied to the film during solvent evaporation.[30,32]

The amplitude and length of buckled structures are measured using three independent techniques: atomic force microscopy in tapping mode (using a MultiMode AFM (Digital Instrument-Veeco)), white-light interferometry (using a Zygo NewView 7200 optical interferometer), and scanning electron microscopy (using a Zeiss 1540XB crossbeam focused ion beam SEM). Each data point in Figure 2c is obtained as an average of amplitude *versus* corresponding length of 20 buckled structures. The error bars in Figure 2c include both the uncertainties in the three measurement techniques and the standard deviation of the 20 measured structures.

Preculture Treatment. After fabrication, all substrates/devices are placed on a glass coverslip to fix the PDMS. The coverslip is sterilized by UV treatment for 30 min and placed in a Petri dish, ready for surface coating. Starting from this step on, every procedure is carried out in a sterile environment.

Surface Coating. Devices are surface-functionalized by 1 mg/mL PDL in various ways to facilitate the uniform or selective adhesion during the cell seeding process. The first step is to activate the surface to favor PDL adhesion. For this purpose, we perform a 2 min oxygen plasma at 100 W RF power. This step is performed for all types of samples investigated in our work, namely, 2D and linear arrays of buckle-delaminated NMs on PDMS, wrinkled NMs on PDMS, and flat NMs on PDMS. Next, the sample surface and the inside of the buckle-delaminated channels are spin-coated with PDL. Samples incorporating buckled-delaminated NM channels on PDMS undergo an additional processing step, namely, a transient oxygen plasma etch at 25 W for 10 s to remove the PDL coating everywhere but inside the buckle-delaminated NMs. We expect that diffusion limitations of the etch vapor through channel inlets results in the PDL coating the inside of channels to remain to form a selective coating to enhance guidance. Wrinkled and flat NM stripes were uniformly coated with PDL or patterned with arrays of PDL lines. The PDL patterning is done by microcontact stamping, which created 8 μm spaced parallel lines, as described previously.[11]

Immunostaining and Fluorescent Imaging. The culture sample for fluorescent imaging is fixed in 4% paraformaldehyde/Krebs/sucrose fixative at pH 7.4 for 30 min. Cultures are then blocked with 10% BSA/PBS, permeabilized in 0.2% Trition X-100/PBS, and labeled with antibodies to tubulin at 1:1000 (YL1/2 clone, Chemicon). Secondary antibodies coupled to Alexa 568 are

used at 1:500, and Alexa 488/phalloidin (Invitrogen) is used to label actin filaments (1:100). Fixed cell cultures are imaged with a Fluoview500 AX70 upright (Olympus, USA) microscope through a 40× water-immersion lens with a 0.8 numerical aperture.

Fabrication and Electrical Characterization of Single Buckled Interconnects. We pattern a 42 nm Si template in a near-checkerboard fashion while on its original SiO_2/handle Si substrate. We use photolithography, e-beam evaporation of a 5/200 nm Cr/Au film, and lift-off to fabricate rectangular contact pads on the NM. After release and transfer of the NM to the PDMS substrate, the sample is treated in acetone for 2 h and rinsed in IPA for 120 s. The NM/PDMS is then exposed to air at room temperature to allow buckle-delaminated interconnects to form between contact pads as the solvent evaporates.[30]

Current−voltage measurements are performed on a probe station using an Agilent/HP4156C semiconductor parameter analyzer. Reproducibility of the measurements is tested by sweeping the bias five consecutive times with alternating polarity for each measured structure. The series resistance of a test device is estimated by measuring the slope of the $I-V$ curve in the ohmic portion. The series resistance depends on the measurement instrument, method of connection, and current path, as this is a two-terminal measurement.

Fabrication of Light-Emitting Buckled Structures. We use e-beam evaporation to deposit a 10 nm a-Si/10 nm SiO/10 nm SiNM on 400 nm a-Ge sacrificial layer on a bulk Si substrate. The a-Ge layer is previously deposited by e-beam evaporation on an RCA-cleaned bulk Si wafer. We use photolithography and reactive ion etching with CF_4/O_2 to pattern the Si/SiO/SiNM in a checkerboard fashion. After rapid thermal annealing for 10 min at 800 °C in forming gas, the NMs are released by selective etching of the Ge film in 31% H_2O_2 at room temperature. We perform dry transfer of the Si/SiO/SiNM onto PDMS. A 2D array of buckle-delaminated structures is obtained after 30 min immersion in acetone followed by a 120 s rinse in IPA and 15 min exposure to air at room temperature.

Photoluminescence Spectroscopy of SiNMs. We perform microphotoluminescence using a LabRAM Aramis (Horiba Jobin Yvon) confocal Raman microscope equipped with an excitation source operating at ∼633 nm. In our measurements, the laser power is attenuated from 6 to ∼0.6 mW focused to approximately 3 μm using a 50× microscope objective lens.

Neural Culturing. All of the cell cultures reported in this paper used E15.5 cortical neurons obtained from Swiss Webster mice, as previously described.[44] Briefly, cortices were dissected. The cells were dissociated by treating with trypsin (0.25%, 15 min, 37 °C), then triturated with a micropipette tip, diluted in plating medium (neurobasal medium with 5% FBS, Hyclone, B27 supplement, 2 mM glutamine, 37.5 mM NaCl, and 0.3% glucose), and plated onto the substrates at low density (3000−10 000 cells/cm^2). After 1 h, the sample was flooded with serum-free medium (plating medium without FBS) and incubated for 5−7 days.

Conflict of Interest: The authors declare no competing financial interest.

Acknowledgment. We thank Tim Gomez for sharing his insights in fluorescent imaging. F.C. thanks Prof. Kevin Turner, Dr. David Grierson, and Dr. Kevin Christ for useful discussions. The fabrication of the nano- and microstructures used in this work was supported by DOE, Grant No. DE-FG02-03ER46028. The cell culture experiments were supported by the Wisconsin Alumni Research Foundation (WARF). F.C. fabricated the structures; F.C. and Y.H. did the experiments; Y.H. and E.D. provided the biological materials; F.C., Y.H., J.W., and M.L. wrote the paper.

Supporting Information Available: Figure S1 illustrates various types/geometries of hard/soft substrates obtained with the approach described in the article. Figure S2 demonstrates the viability of neurons on SiNM/PDMS after 14 days *in vitro*. This material is available free of charge *via* the Internet at http://pubs.acs.org.

REFERENCES AND NOTES

1. Pearce, T. M.; Williams, J. C. Microtechnology Meet Neurobiology. *Lab Chip* **2007**, *7*, 30–40.
2. *Culturing Nerve Cells*; Goslin, K.; Banker, G., Eds.; MIT Press: Cambridge, MA, 1991; pp 251−281.
3. Taylor, D. M.; Tillery, S. H.; Schwartz, A. B. Direct Cortical Control of 3D Neuroprosthetic Devices. *Science* **2002**, *7*, 1829–1832.
4. *Toward Replacement Parts for the Brain: Implantable Biomimetic Electronics as Neural Prostheses*; Berger, T. W., Glanzman, L. D., Eds; MIT Press: Cambridge, MA, 2005.
5. Soe, A.; Nahavandi, S.; Khoshmanesh, K. Neuroscience Goes on a Chip. *Biosens. Bioelectron.* **2012**, *35*, 1–13.
6. Park, J. W.; Vahidi, B.; Taylor, A. M.; Rhee, S. W.; Jeon, N. L. Microfluidic Culture Platform for Neuroscience Research. *Nat. Protoc.* **2006**, *1*, 2128–2136.
7. Thompson, M.; Cheran, L.; Sadeghi, S. *Sensor Technology in Neuroscience*; RSC Publishing: London, 2013.
8. Robinson, J. T.; Jorgolli, M.; Shalek, A. K.; Yoon, M. H.; Gertner, R. S.; Park, H. Vertical Nanowire Electrode Arrays as a Scalable Platform for Intracellular Interfacing to Neuronal Circuits. *Nat. Nanotechnol.* **2012**, *7*, 180–184.
9. Vansteensel, M. J.; Hermes, D.; Aarnoutse, E. J.; Bleichner, M. G.; Schalk, G.; van Rijen, P. C.; Leijten, F. S.; Ramsey, N. F. Brain−Computer Interfacing Based on Cognitive Control. *Ann. Neurol.* **2010**, *67*, 809–816.
10. Vitzthum, I.; Chen, X.; Kintner, D. B.; Huang, Y.; Chiu, S. Y.; Williams, J. C.; Sun, D. Study of Na^+/H^+ Exchange-Mediated pHi Regulations in Neuronal Soma and Neurites in Compartmentalized Microfluidic Devices. *Integr. Biol.* **2010**, *2*, 58–64.
11. Hart, S. R.; Huang, Y.; Fothergill, T.; Lumbard, D. C.; Dent, E. W.; Williams, J. C. Adhesive Micro-line Periodicity Determines Guidance of Axonal Outgrowth. *Lab Chip* **2013**, *13*, 562–569.
12. Huang, Y.; Agrawal, B.; Clark, P. A.; Williams, J. C.; Kuo, J. S. Evaluation of Cancer Stem Cell Migration Using Compartmentalizing Microfluidic Devices and Live Cell Imaging. *J. Vis. Exp.* **2011**, *58*, e3297.
13. Huang, Y.; Williams, J. C.; Johnson, S. M. Brain Slice on a Chip: Opportunities and Challenges of Applying Microfluidic Technology to Intact Tissue. *Lab Chip* **2012**, *12*, 2103–2117.
14. Moore, S. W. Stretchy Proteins on Stretchy Substrates: The Important Elements of Integrin-Mediated Rigidity Sensing. *Dev. Cell* **2010**, *19*, 194–206.
15. *CRC Materials Science and Engineering Handbook*; Shackelford, J. F., Alexander, W., Eds.; CRC Press: Boca Raton, FL, 2000.
16. Discher, D. E.; Janmey, P.; Wang, Y. Tissue Cells Feel and Respond to the Stiffness of Their Substrate. *Science* **2005**, *310*, 1139–1143.
17. Janmey, P. A.; McCulloch, C. A. Cell Mechanics: Integarting Cell Response to Mechanical Stimuli. *Annu. Rev. Biomed. Eng.* **2007**, *9*, 1–34.
18. Kerstein, P. C.; Jacques-Fricke, B. T.; Rengifo, J.; Mogen, B. J.; Williams, J. C.; Gottlieb, P. A.; Sachs, F.; Gomez, T. M. Mechanosensitive TRPC1 Channels Promote Calpain Proteolysis of Talin To Regulate Spinal Axon Outgrowth. *J. Neurosci.* **2013**, *33*, 273–285.
19. Bazaka, K.; Jacob, M. V. Implantable Devices: Issues and Challenges. *Electronics* **2013**, *2*, 1–34.
20. Williams, J. C.; Rennaker, R. L.; Kipke, D. R. Stability of Chronic Multichannel Neural Recordings: Implications for a Long-Term Neural Interface. *Neurocomputing* **1999**, *26*, 1069–1076.
21. Cogan, S. Neural Stimulation and Recording Electrodes. *Annu. Rev. Biomed. Eng.* **2008**, *10*, 275–309.
22. Boyden, E. S.; Zhang, F.; Bamberg, E.; Nagel, G.; Deisseroth, K. Millisecond-Timescale, Genetically Targeted Optical Control of Neural Activity. *Nat. Neurosci.* **2005**, *8*, 1263–1268.
23. Fromhertz, P. In *Nanoelectronics and Information Technology*; Waiser, R., Ed.; Wiley-VCH: Weinheim, Germany, 2003; pp 781−810.
24. Rutten, W. L. Selective Electrical Interfaces with the Nervous System. *Annu. Rev. Biomed. Eng.* **2002**, *4*, 407–452.
25. Kotov, N. A.; Winter, J. O.; Clements, I. P.; Jan, E.; Timko, B. P.; Campidelli, S.; Pathak, S.; Mazzatenta, A.; Lieber, C. M.;

Prato, M.; *et al.* Nanomaterials for Neural Interfaces. *Adv. Mater.* **2009**, *21*, 3970–4004.
26. Cavallo, F.; Grierson, D. S.; Turner, K. T.; Lagally, M. G. "Soft Si": Effective Stiffness of Crystalline Supported Nanomembranes. *ACS Nano* **2011**, *5*, 5400–5407.
27. Scott, S. A.; Lagally, M. G. Elastically Strain Sharing Nanomembranes: Flexible and Transferable Strained Silicon and Silicon–Germanium Alloy. *J. Phys. D: Appl. Phys.* **2007**, *40*, R75–R92.
28. Cavallo, F.; Lagally, M. G. Semiconductors Turn Soft: Inorganic Nanomembranes. *Soft Matter* **2010**, *6*, 439–455.
29. Rogers, J. A.; Lagally, M. G.; Nuzzo, R. G. Semiconductor Nanomembranes: Synthesis, Assembly and Applications. *Nature* **2011**, *477*, 45–53.
30. Cavallo, F.; Turner, K. T.; Lagally, M. G. Facile Fabrication of Ordered Crystalline-Semiconductor Microstructures on Compliant Substrates. *Adv. Funct. Mater.* **2014**, *24*, 1730–1737.
31. Lee, J. N.; Park, C.; Whitesides, G. M. Solvent Compatibility of Poly(dimethylsiloxane)-Based Microfluidic Devices. *Anal. Chem.* **2003**, *75*, 6544–6554.
32. Mei, H.; Huang, R.; Chung, J. Y.; Stafford, C. M.; Yu, H. H. Buckling Modes of Elastic Thin Films on Elastic Substrates. *Appl. Phys. Lett.* **2007**, *90*, 151902.
33. Yavin, E.; Yavin, Z. Attachment and Culture of Dissociated Cells from Rat Embryo Cerebral Hemispheres on Polylysine-Coated Surface. *J. Cell. Biol.* **1974**, *62*, 540–546.
34. Yu, M.; Huang, Y.; Ballweg, J.; Shin, H.; Huan, M.; Savage, D. E.; Lagally, M. G.; Dent, E. W.; Blick, R. H.; Williams, J. C. Semiconductor Nanomembrane Tubes: Three-Dimensional Confinement for Controlled Neurite Outgrowth. *ACS Nano* **2011**, *5*, 2447–2457.
35. Schulze, S.; Huang, G.; Krause, M.; Aubyn, D.; Quinones, V. A.; Schmidt, C. K.; Schmidt, O. G. Morphological Differentiation of Neurons on Microtopographic Substrates Fabricated by Rolled-up Nanotechnology. *Adv. Eng. Mater.* **2010**, *12*, B558–B564.
36. Rowe, L.; Almasri, M.; Lee, K.; Fogleman, N.; Brewer, G. J.; Nam, Y.; Wheeler, B. C.; Vukasinovic, J.; Glezer, A.; Frazier, A. B. Active 3-D Microscaffold System with Fluid Perfusion for Culturing *In Vitro* Neuronal Networks. *Lab Chip* **2007**, *7*, 475–482.
37. Funch, P. G.; Faber, D. S. Measurement of Myelin Sheath Resistances: Implications for Axonal Conduction and Pathophysiology. *Science* **1984**, *225*, 538–540.
38. Li Jeon, N.; Baskaran, H.; Dertinger, S. K.; Whitesides, G. M.; Van de Water, L.; Toner, M. N. Neutrophil Chemotaxis in Linear and Complex Gradients of Interleukin-8 Formed in a Microfabricated Device. *Nat. Biotechnol.* **2002**, *20*, 826–830.
39. Khriachtchev, L.; Ossicini, S.; Iacona, F.; Gourbilleau, F. Silicon Nanoscale Materials: From Theoretical Simulations to Photonic Applications. *Int. J. Photoenergy* **2012**, *2012*, 872576.
40. *Silicon Nanocrystals: Fundamentals, Synthesis and Applications*; Pavesi, L., Turan, R., Eds.; Wiley-VCH: Weinheim, Germany, 2010.
41. Zhang, F.; Prigge, M.; Beyrière, F.; Tsunoda, S. P.; Mattis, J.; Yizhar, O.; Hegemann, P.; Deisseroth, K. Red-Shifted Optogenetic Excitation: A Tool for Fast Neural Control Derived from Volvox Carteri. *Nat. Neurosci.* **2008**, *11*, 633–635.
42. Lyn, J. Y.; Knutsen, P. M.; Muller, A.; Kleinfeld, D.; Tsien, R. Y. ReaChR: A Red-Shifted Variant of Channelrhodopsin Enables Deep Tanscranial Optogenetic Excitation. *Nat. Neurosci.* **2013**, *16*, 1499–1508.
43. Song, C.; Huang, R.; Wang, X.; Guo, Y.; Song, J. Tunable Red Light Emission from a-Si:H/a-SiNx Multilayers. *Opt. Mater. Express* **2013**, *3*, 664–670.
44. Viesselmann, C.; Ballweg, J.; Lumbard, D.; Dent, E. W. Nucleofection and Primary Culture of Embryonic Mouse Hippocampal and Cortical Neurons. *J. Vis. Exp.* **2011**, *47*, e2373.